




Runt related transcription factor-1 plays a central role in vessel co-option of colorectal cancer liver metastases

Miran Rada¹, Audrey Kapelanski-Lamoureux¹, Stephanie Petrillo¹, Sébastien Tabariès ², Peter Siegel ², Andrew R. Reynolds³, Anthoula Lazaris ¹ & Peter Metrakos ¹✉

Colorectal cancer liver metastasis (CRCLM) has two major histopathological growth patterns: angiogenic desmoplastic and non-angiogenic replacement. The replacement lesions obtain their blood supply through vessel co-option, wherein the cancer cells hijack pre-existing blood vessels of the surrounding liver tissue. Consequentially, anti-angiogenic therapies are less efficacious in CRCLM patients with replacement lesions. However, the mechanisms which drive vessel co-option in the replacement lesions are unknown. Here, we show that Runt Related Transcription Factor-1 (RUNX1) overexpression in the cancer cells of the replacement lesions drives cancer cell motility via ARP2/3 to achieve vessel co-option. Furthermore, overexpression of RUNX1 in the cancer cells is mediated by Transforming Growth Factor Beta-1 (TGFβ1) and thrombospondin 1 (TSP1). Importantly, RUNX1 knockdown impaired the metastatic capability of colorectal cancer cells *in vivo* and induced the development of angiogenic lesions in liver. Our results confirm that RUNX1 may be a potential target to overcome vessel co-option in CRCLM.

¹Cancer Research Program, McGill University Health Centre Research Institute, Montreal, QC, Canada. ²Rosalind and Morris Goodman Cancer Research Centre, McGill University, Montreal, QC, Canada. ³Oncology R&D, AstraZeneca, Cambridge, United Kingdom. ✉email: peter.metrakos@mcgill.ca

Colorectal cancer (CRC) is the third most commonly diagnosed cancer in the world and ranking the second leading cause of cancer-related deaths in developed countries¹. Since the majority of the intestinal mesenteric drainage enters the hepatic portal venous system, CRC metastases often spread to the liver, which is a major cause of mortality^{2,3}. Currently, ablation with surgical resection is considered the only curative option resulting in 5-year survival rates of up to 50%. However, surgical treatment is not possible in 80% of colorectal cancer liver metastasis (CRCLM) cases and the patients are left with palliative options, mainly consisting of systemic treatment with palliative intent^{2,4}.

Angiogenesis has been reported as an essential step in the growth of metastatic tumors, which is driven by vascular endothelial growth factor-A (VEGF-A)^{5,6}. Therefore, numerous anti-angiogenic agents targeting VEGF signaling (e.g., Bevacizumab, Regorafenib, Aflibercept) combined with chemotherapy have been identified as an approved treatment in CRCLM patients to extend progression-free and/or overall survival^{7–9}. However, a limited therapeutic benefit to overall survival (OS) has been observed¹⁰. The mechanisms that limit the therapeutic efficacy of anti-angiogenic therapy in patients are still unclear. One of the potential mechanisms that could explain resistance to anti-angiogenesis therapy is vessel co-option, a mechanism by which tumors obtain a blood supply without angiogenesis by exploiting pre-existing vasculature^{9,11–13}. Since the tumor is co-opting the liver's pre-existing vessels, anti-angiogenic treatment may have only a limited effect in vessel co-opting tumors. Vessel co-option has been reported in different cancers, for instance, liver metastases¹⁴, non-small cell lung cancer¹⁵, lung metastases^{16,17}, lymph node metastasis^{18,19} and hepatocellular carcinoma²⁰. Recent studies suggested two major distinct histopathological growth patterns (HGP) of CRCLM lesions including desmoplastic HGP (DHGP) and replacement HGP (RHGP)^{21,22}. DHGP lesions are characterized by a desmoplastic stromal layer that physically separates the cancer cells from the normal liver parenchyma. The cancer cells in DHGP lesions obtain their blood supply through angiogenesis^{14,21,23}. However, the cancer cells in RHGP lesions infiltrate the liver parenchyma and replace the hepatocytes near the tumor periphery to co-opt pre-existing liver sinusoidal vessels instead of promoting angiogenesis^{14,21,24}. Indeed, poor responses to anti-angiogenic therapy combined with chemotherapy have been reported in CRCLM patients with RHGP lesions compared to patients with DHGP lesions who achieve a better response to the same therapy^{11,12,14,24,25}. It is worth mentioning that similar results were observed in breast²⁶, uveal melanoma²⁷, and pancreatic²⁸ liver metastases.

Accumulating evidence suggests that cancer cell motility plays a pivotal role in the process of vessel co-option in various cancers^{9,14,20,29}. Accordingly, Kuczynski et al.²⁰ demonstrated upregulation of pathways involved in cancer cell motility and invasion in vessel co-opting hepatocellular carcinomas, such as epithelial-mesenchymal transition (EMT), STAT3 and Wnt/ β -catenin signaling. The Actin-related protein 2/3 complex (ARP2/3) complex has also been implicated in tumor invasion, and a study from our group showed a positive correlation between ARP2/3 overexpression in cancer cells and CRCLM vessel co-option, and that ARP2/3 knockdown resulted in the conversion of CRCLM lesions with a vessel co-option phenotype to angiogenic lesions *in vivo*¹⁴. However, the molecular mechanisms by which the expression of ARP2/3 is upregulated in cancer cells are poorly understood.

The aim of this study was to understand the molecular mechanisms of vessel co-option in CRCLM. Herein, we identified RUNX1 as a key player in vessel co-option by regulating motility and EMT in cancer cells.

Results

RUNX1 is overexpressed in vessel co-opting CRCLM tumors. Our team previously reported ARP2/3 as a key mediator of vessel co-option in CRCLM¹⁴. The ARP2/3 complex is a stable multi-protein complex composed of seven subunits including ARP2 (ACTR2), ARP3, ARPC1 (p41), ARPC2 (p31), ARPC3 (p21), ARPC4 (p20), and ARPC5 (p16)³⁰. Runt Related Transcription Factor-1 (RUNX1) is among the transcriptional factors that control the expression levels of ARP2/3^{31–33}. It regulates the expression of various ARP2/3 subunits, such as ARPC1, ARPC2, and ARPC3³⁴. RUNX1 is a member of the RUNX transcription factor family³⁵. An abnormal elevation of RUNX1 has been reported in various cancers, for instance, breast cancer, colorectal cancer, pancreatic cancer, and brain cancer^{36–38}. RUNX1 occupied thousands of genomic regions that corresponded to genes involved in tumor progression and angiogenesis^{37,38}.

To address the role of RUNX1 in CRCLM vessel co-option, we examined the protein levels of RUNX1 in various CRCLM samples. It is worth mentioning that most of the CRCLM tumors are heterogeneous with a mixture of desmoplastic, replacement, and pushing^{14,39}. Thus, the ratio of desmoplastic or replacement HGP was quantified in each specimen by a histopathologist following the published consensus guidelines for scoring the HGP²². Firstly, we evaluated the expression levels of RUNX1 in frozen sections of desmoplastic HGP and replacement HGP chemo-naïve CRCLM lesions comparing to distal normal liver tissue. As shown in Fig. 1a, RUNX1 expression was increased in replacement lesions comparing to desmoplastic lesions. Interestingly, we noticed that the lesion with a higher percentage of replacement HGP expressed higher levels of RUNX1. Next, we used immunohistochemical (IHC) staining to further validate our results, which again demonstrated significant overexpression of RUNX1 in cancer cells of replacement lesions compared to desmoplastic (Fig. 1b). Positive RUNX1 staining was quantified using Aperio software^{11,12,40}. Similar results were demonstrated in CRCLM specimens from patients treated with combined chemotherapy and bevacizumab (chemo + bev) as shown in Supplementary Fig. 1a. Interestingly, RUNX1 expression is uniformly higher in the cancer cells adjacent to liver tissue. To gain insight into RUNX1 biology, we investigated the expression of various genes, that have been reported to be transcriptionally regulated by RUNX1, in CRCLM lesions using our RNA-seq data that was recently published (GSE151165)⁴⁰, as shown in Fig. 1c. We noticed that the majority of RUNX1 target genes were upregulated in replacement type CRCLM sections. The genes linked to EMT (e.g., *CDH2*, *CDH16*, *SNAI1*, *SNAI2*, and *VIM*)^{41–43} and cell motility (*ARPC1b*, *ARPC2*, and *ARPC3*)⁴⁴ are among RUNX1 target genes that were upregulated in replacement lesions. However, the upregulation of some of these genes was not statistically significant. Thus, to validate some of these genes we stained CRCLM sections for E-Cadherin or ARP2/3. In-vessel co-opting lesions, we observed low expression of E-Cadherin in the cancer cells adjacent to liver tissue in chemo-naïve and chemo+bev samples (Fig. 1d and Supplementary Fig. 1b). Conversely, the expression levels of ARP2/3 were almost two-fold higher in the cancer cells at the periphery of vessel co-opting lesions comparing to their counterparts in angiogenic lesions (Fig. 1e). Contrary to RUNX1 expression, we did not demonstrate any major difference in the expression of ARP2/3 between central and peripheral tumors in co-opted lesions. These observations suggest that although RUNX1 is a transcriptional factor of ARP2/3^{31–33}, there are other possible proteins that regulate ARP2/3 expression that need to be explored in the future. Of note, previous investigations reported that low expression of E-cadherin accompanied by high expression of ARP2/3 contribute to EMT⁴⁵ and motility⁴⁶ in the cancer cells. Altogether, our data

Fig. 1 RUNX1 overexpressed in the replacement colorectal cancer liver metastasis lesions. **a** Western blot of RUNX1 in distal normal liver (control) and chemo-naïve CRCLM cancer cells (left panel). The right panel represents the intensity of the bands ($n = 3$) that were determined using ImageJ software. **b** Immunohistochemistry staining of chemo-naïve CRCLM lesions using an anti-RUNX1 antibody (left panel). Right panels show the positivity [total number of positive pixels/total number of pixels] that measured in RHGP ($n = 5$) and DHGP ($n = 5$) specimens using an optimized Aperio algorithm (mean + SD). C-RHGP Central tumor cells in RHGP lesions, P-RHGP Peripheral tumor cells in RHGP lesions, C-DHGP Central tumor cells in DHGP, P-DHGP Peripheral tumor cells in DHGP lesions. **c** Heatmap showing the expression of RUNX1 target genes in DHGP ($n = 6$) and RHGP ($n = 6$) CRCLM tumors. Red representing the highest levels of expression and blue representing the lowest levels of expression. **d, e** Immunohistochemistry staining of chemo-naïve CRCLM lesions with E-cadherin or ARP2/3 antibody, respectively (top panel). Bottom panels show the positivity [total number of positive pixels/total number of pixels] that measured in RHGP ($n = 5$) and DHGP ($n = 5$) specimens using an optimized Aperio algorithm (mean + SD). C-RHGP Central tumor cells in RHGP lesions, P-RHGP Peripheral tumor cells in RHGP lesions, C-DHGP=Central tumor cells in DHGP, P-DHGP Peripheral tumor cells in DHGP lesions. Data are presented as the mean \pm SD.

significant elevation in TGF β 1 expression in vessel co-opting type CRCLM lesions relative to desmoplastic (Fig. 2a and Supplementary Fig. 2a). Importantly, TGF β 1 staining was significantly higher ($p < 0.0001$) in hepatocytes at the tumor-liver interface where the hepatocytes of the normal adjacent liver and cancer cells in the replacement HGP are in very close proximity. To identify unequivocally in which tissue compartment the expression of TGF β 1 is upregulated, we performed fluorescence in situ hybridization (FISH) assay for TGF β 1 combined with cancer cell-specific (anti-Cytokeratin 20) staining. The results demonstrated that TGF β 1 is mainly expressed in the adjacent normal liver parenchyma (most likely hepatocytes) in CRCLM lesions and not in the cancer cells (Fig. 2b). We further confirmed these results using the FISH assay for TGF β 1 combined with Hepatocyte Specific Antigen (HSA) staining (Supplementary Fig. 2b). Accordingly, any positive staining of adjacent cancer cells for TGF β 1 is most likely due to their uptake of the secreted TGF β 1 from the liver parenchyma (hepatocytes) rather than an up-regulated expression of TGF β 1 in cancer cells.

We also demonstrated upregulation of the TGF β 1 receptor II (TGF β R2) in chemo-naïve replacement HGP tumors (Fig. 2c). SMAD2 and p38 represent canonical and non-canonical TGF β 1 signaling pathways, respectively⁵⁰. We observed phosphorylated SMAD2 (S465/467) and phosphorylated p38 (T180/Y182) at the tumor-liver interface of RHGP lesions, but not at the tumor-liver interface of DHGP lesions (Supplementary Fig. 3). Remarkably, the adjacent hepatocytes of co-opted lesions also expressed high levels of phosphorylated SMAD2 (S465/467) and phosphorylated p38 (T180/Y182), indicating that TGF β 1 in the adjacent hepatocytes of co-opted lesions may participate in furnishing a favorable environment for cancer cells to establish vessel co-option via multiple mechanisms. These mechanisms might include inducing hepatocyte displacement by cancer cells^{14,51} or overexpression of Angiopoietin-1 (Ang1) in adjacent hepatocytes¹². Our lab is currently examining these hypotheses.

Next, we asked whether RUNX1 expression in cancer cells was affected by the presence of TGF β 1 or TGF β R2 in vitro. Firstly, we treated CRC (HT29) cells with recombinant TGF β 1. RUNX1 was strongly expressed upon exposure to TGF β 1 (Fig. 2d). This effect of TGF β 1 in RUNX1 expression was inhibited in the cancer cells expressing shRNA against TGF β R2 (Fig. 2e). Similar results were reproduced using TGF β R2 inhibitor (ITD1)⁵² in both HT29 and SW620 colorectal cancer cells (Fig. 2f). Taken together, these experiments indicate that TGF β 1 signaling can induce RUNX1 expression in cancer cells through TGF β R2.

RUNX1 modulates TGF β 1 expression in hepatocytes through TSP1. To identify the role of cancer cells in TGF β 1 expression by hepatocytes, we examined the expression of TGF β 1 in IHH hepatocytes in the presence or absence of cancer cells (HCT116, HT29, LS174, LS180, SW620, and COLO320dm) using insert co-culturing approach (Fig. 3a). IHH cells are immortalized human

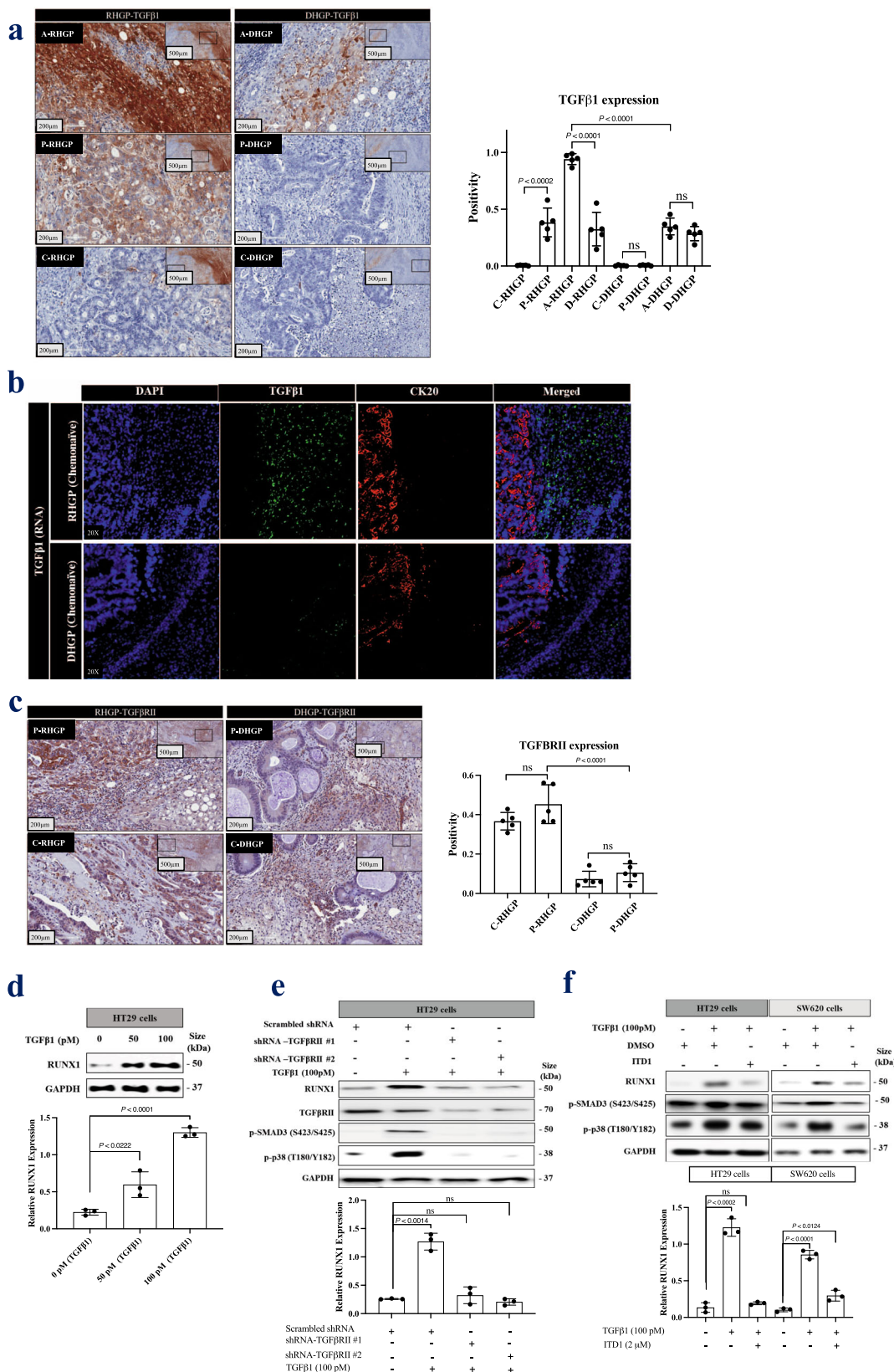
hepatocytes that retained several differentiated features of normal hepatocytes^{53–55}. As shown in Fig. 3b, co-culturing hepatocytes with various colorectal cancer cell lines enhanced TGF β 1 expression in the hepatocytes. We further confirmed these results using immunofluorescence staining (Fig. 3c).

We speculated that the expression of TGF β 1 in hepatocytes could be induced by secreted factors from the cancer cells, which are under the transcription control of RUNX1. To test this hypothesis, we knocked down RUNX1 in HT29 and SW620 cancer cells followed by co-culturing with hepatocytes (IHH cells). As shown in Figs. 3d and 3e, the absence of RUNX1 in the co-cultured cancer cells resulted in lower expression of TGF β 1 in hepatocytes. These results suggest that RUNX1 plays an essential role in the crosstalk between cancer cells and hepatocytes through its target genes.

Thrombospondin-1 (TSP1) is a secreted protein, encoded by *THBS1*, which is a target gene of RUNX1^{56,57}. Soto-Pantoja et al. have reported TSP1 as a regulator of TGF β 1 expression in TSP1-null mice that failed to express TGF β 1⁵⁸. Other investigations have also identified TSP1 as an activator of TGF β 1⁵⁹. Our results suggested a positive correlation between TSP1 and RUNX1 expression in HT29 and SW620 colorectal cancer cells (Figs. 3f and 3g). We then turned our attention to those RUNX1 target genes that are upregulated in RNA-seq data that are shown in Fig. 1c. We noticed that the expression of TSP1 (*THBS1*) is higher in replacement CRCLM tumors in comparison to their desmoplastic counterparts. In both chemo-naïve (Fig. 3h) and chemo + bev CRCLM specimens, our IHC data suggested a significant increase of TSP1 on the protein levels in replacement co-opted lesions (Supplementary Fig. 4a).

CD36 is among TSP1 receptors^{60–62} that mediate TSP1-TGF β 1 interaction^{63–65}. We confirmed that CD36 acts as a receptor of TSP1 in hepatocytes in vitro using co-immunoprecipitation assay (Supplementary Fig. 4b). Intriguingly, immunohistochemical results showed overexpression of CD36 in hepatocytes adjacent to the cancer cells of replacement lesions in chemo-naïve CRCLM sections (Supplementary Fig. 4c). Therefore, we hypothesized that the crosstalk between RUNX1 and TGF β 1 may be mediated by TSP1. To address this, we first treated IHH hepatocytes with different concentrations of recombinant TSP1. Exposing IHH cells to recombinant TSP1 resulted in higher expression of TGF β 1 (Fig. 3i). The effect of TSP1 on TGF β 1 expression by hepatocytes was further ascertained by generating TSP1-silenced HT29 and LS174 colorectal cancer cells (Supplementary Fig. 4d) and co-culturing them with IHH cells. The cancer cells with silenced-TSP1 were failed in stimulating TGF β 1 expression in hepatocytes (Fig. 3j).

To further examine the molecular mechanisms explaining the signaling crosstalk between hepatocytes and cancer cells; we conducted a co-culturing experiment between hepatocytes and cancer cells followed by Western blotting to evaluate RUNX1 expression in the cancer cells. Co-culturing hepatocytes with



colorectal cancer (HT29, SW620, and COLO320dm) cells resulted in a dramatic increase of RUNX1 protein levels (Fig. 3k, left panel). This might be due to the presence of TGFβ1 in the conditioned media of co-cultured cells (Fig. 3k, right panel). We repeated a similar experiment by co-culturing HT29 cancer cells with hepatocytes in the presence of LSKL (Leucine-Serine-Lysine-

Leucine), an inhibitor of TSP1-mediated TGFβ1 activation^{66,67}. The expression of RUNX1 was reduced to normal levels upon LSKL1 treatment (Fig. 3l). In summary, these data suggest signaling crosstalk between hepatocytes and cancer cells that regulates the expression of both TGFβ1 and RUNX1, which is orchestrated through TSP1.

Fig. 2 TGF β 1 regulates RUNX1 expression in cancer cells through TGF β RII. **a** Left panel represents immunohistochemical staining of RHGP ($n = 5$) and DHGP ($n = 5$) chemo-naïve CRCLM specimens using TGF β 1 antibody. The right panel shows the positivity [total number of positive pixels/total number of pixels] was measured using an optimized Aperio algorithm (mean + SD). **b** Fluorescence in situ hybridization (FISH) for TGF β 1 mRNA (green) expression in chemo-naïve CRCLM lesions overlapped with CK20 (cytokeratin 20, red) antibody. **c** The left panel shows immunohistochemistry staining of chemo-naïve CRCLM lesions with TGF β RII antibody. The right panel shows the positivity [total number of positive pixels/total number of pixels] was measured using an optimized Aperio algorithm (mean + SD). **d** Western blot of RUNX1 in HT29 cancer cells upon treatment with recombinant TGF β 1 for 24 h (top panel). **e** Western blot of RUNX1 and TGF β RII in HT29 cancer cells expressing either scrambled shRNA or shRNA against TGF β RII in the presence or absence of recombinant TGF β 1 for 24 h (top panel). **f** Western blot of RUNX1 in HT29 and SW620 cancer cells in the presence or absence of recombinant TGF β 1 individually or TGF β 1 with 2 μ M of TGF β RII inhibitor (ITD1) for 24 h (top panel). The bottom panels represent the intensity of the bands ($n = 3$). C-RHGP Central tumor cells in RHGP lesions, P-RHGP Peripheral tumor cells in RHGP lesions, A-RHGP Adjacent hepatocytes to tumor lesion in RHGP, D-RHGP Distal hepatocytes to tumor lesion in RHGP, C-DHGP Central tumor cells in DHGP, P-DHGP Peripheral tumor cells in DHGP lesions, A-DHGP Adjacent hepatocytes to tumor lesion in DHGP, D-DHGP Distal hepatocytes to tumor lesion in DHGP. Data are presented as the mean \pm SD.

RUNX1 inhibition suppresses TGF β 1-driven EMT and motility in colorectal cancer cells in vitro. TGF β 1 plays a crucial role in colorectal cancer cells EMT and cell invasion⁶⁸. To find out if RUNX1 can modulate TGF β 1 function in these processes, we performed various in vitro experiments and treated cancer cells with either recombinant TGF β 1 or co-cultured with hepatocyte (IHH) cells, upon RUNX1 inhibition.

RUNX1 binding to Core-Binding Factor Subunit Beta (CBF β) has been reported, which stabilizes the RUNX-DNA interaction allosterically⁶⁹. Interestingly, immunohistochemical staining showed positive staining for CBF β in CRCLM sections as well (Supplementary Fig. 5a). Ro5-3335 inhibits CBF β binding with RUNX1 which then blocks RUNX1 transcriptional activity^{35,70}. Therefore, we used Ro5-3335 as a RUNX1 inhibitor for our in vitro experiments.

To identify the role of RUNX1 in TGF β 1-driven motility and EMT in colorectal cancer cells, we treated HT29 and LS174 colorectal cancer cells with TGF β 1 in the presence or absence of Ro5-3335 for 24 h followed by immunoblotting using anti-ARP2/3 and anti-vimentin antibodies representing cancer cell invasion⁷¹ and EMT⁷², respectively. As shown in Fig. 4a,

TGF β 1-dependent ARP2/3 and vimentin expression in cancer cells were attenuated in the presence of RUNX1 inhibitor (Ro5-3335). Similar results were obtained using immunofluorescence staining in HT29 (Fig. 4b) and COLO320dm cancer cells (Supplementary Fig. 5b). These data were further validated when RUNX1 function in HT29 cancer cells was suppressed using RUNX1 shRNA (Fig. 4c).

RUNX1 has been reported as a transcriptional factor for different genes including Ang1⁷³ and IGFBP3⁷⁴, encoding angiopoietin-1 and Insulin-like growth factor-binding protein-3 proteins, respectively. Both Ang1⁷⁵ and IGFBP3⁷⁶ are known as angiogenesis inhibitors. Therefore, we questioned whether RUNX1 and TGF β 1 are involved in the expression of these genes in CRC cells. Our immunofluorescence staining demonstrated upregulation of both proteins in CRC cells upon exposure to recombinant TGF β 1, while the effect of TGF β 1 was impaired in the presence of RUNX1 inhibitor (Ro5-3335) (Supplementary Fig. 6a and 6b). We recently published a paper¹² demonstrating that knocking out of Ang1 in the host liver significantly induces the formation of desmoplastic CRCLM lesions. However, major gaps in our knowledge need fulfillment in future studies regarding the impact of Ang1 and/or IGFBP3 overexpression in cancer cells in the establishment of co-opted tumor lesions in the liver.

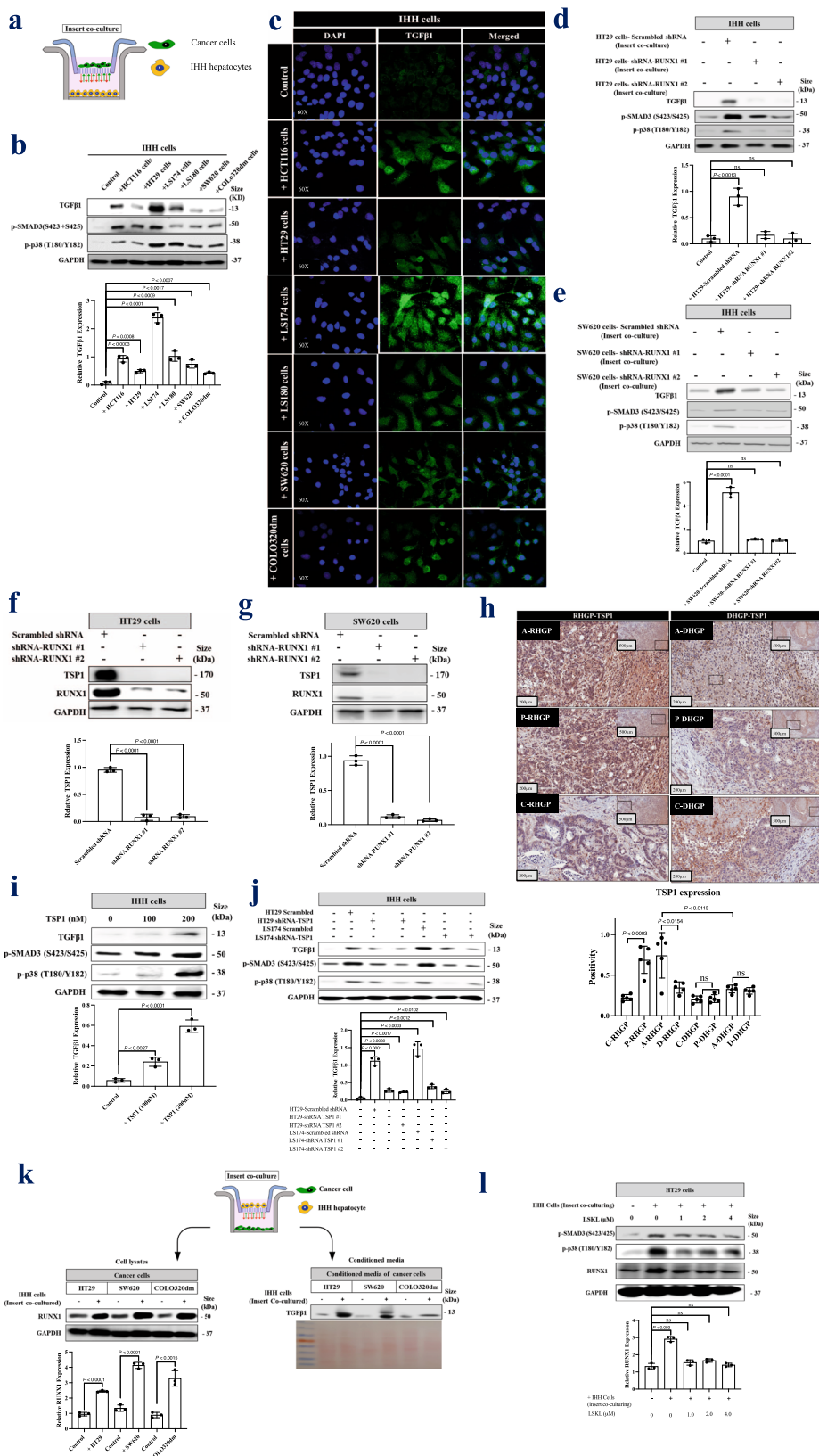
To evaluate the effect of RUNX1 in TGF β 1-mediated invasion in colorectal cancer cells, we conducted a wound-healing assay using three different colorectal cancer cell lines including HT29, SW620, or COLO320dm (Fig. 4d). We used recombinant TGF β 1 either individually or in combination with RUNX1 inhibitor

(Ro5-3335) to treat the cancer cells for 24 h. The TGF β 1-treated cells showed higher levels of wound healing, while the presence of RUNX1 inhibitor suppressed this effect. Consistently, silencing RUNX1 in HT29 cells by shRNA attenuated the function of TGF β 1 in wound healing (Supplementary Fig. 6c). Importantly, the ectopic expression of RUNX1 restored both TGF β 1-dependent ARP2/3 expression (Fig. 4e) and wound healing (Fig. 4f) that were inhibited by RUNX1 depletion. Taken together, these results implied that proper RUNX1 function is necessary for TGF β 1 signaling in EMT and cell invasion in colorectal cancer cells.

RUNX1 knockdown in cancer cells promotes the formation of angiogenic desmoplastic CRCLM lesions in vivo.

To gain a better understanding of the effects of RUNX1 in vessel co-option and identify its importance in developing or maintaining vessel co-opted CRCLM tumors in vivo, we used both intrasplenic and intrahepatic xenograft mouse models. Firstly, we injected SCID Beige mice intrasplenically with HT29 cancer cells expressing scrambled or RUNX1 shRNA. The RUNX1-deficient HT29 cancer cells showed lower capability for liver metastasis and formation of replacement vessel co-option lesions comparing to control (Figs. 5a and 5b). Accordingly, all the mice (3/3) that injected with control HT29 cells were developed liver metastasis, while 83% (5/6) of the mice that injected RUNX1-depleted HT29 cells lacked liver metastasis. Significantly, all developed metastatic lesions in the control group had replacement histological growth patterns, while 50% of the lesions in the one mouse that developed liver metastases in the shRNA-RUNX1 group were desmoplastic type. Immunohistochemical staining was used to determine the expression levels of RUNX1, ARP2/3, TSP1 (Fig. 5b, d), and TGF β 1 (Supplementary Fig. 7) in tumor sections, which we found lower levels of their expression in RUNX1-knockdown specimens than their control counterparts.

To further elucidate the role of RUNX1 in the development of vessel co-option in vivo, HT29 cancer cells expressing scrambled or RUNX1 shRNA were injected into SCID Beige mice intrahepatically. After 6 weeks, the tumors were analyzed for histopathological growth patterns. A dramatic increase in the ratio of desmoplastic lesions was detected in mice injected with RUNX1-depleted cancer cells comparing to controls (Figs. 5c and 5d). We also noticed a reduction in the size and number of lesions in the absence of RUNX1 in injected cancer cells. Since RUNX1 knockdown reduces cell proliferation in HT29 colorectal cancer cells (Supplementary Fig. 8), the size reduction in the RUNX1-depleted tumors may be caused by lower cell proliferation of the cancer cells. Overall, these results confirm the governing role of RUNX1 in the development or maintenance of the vessel co-opting replacement CRCLM lesions.



Discussion

Colorectal cancer liver metastasis represents one of the most challenging tumors to treat, and these tumors are often resistant to anti-angiogenic therapy¹⁰. Different angiogenic and non-angiogenic compensatory pathways contribute to the adaptation

of tumors to anti-angiogenic drugs. Vessel co-option⁹, increased pericyte coverage⁷⁷, vasculogenic mimicry⁷⁸, autophagy⁷⁹, lysosomal sequestration⁸⁰, and glycosylation-dependent⁸¹ resistance are among the mechanisms that may contribute to anti-angiogenic therapy resistance^{10,82,83}. In CRCLM, we believe

Fig. 3 RUNX1 forms a positive feedback loop with TGFβ1 through TSP1. **a** Schematic of experimental design. **b** Western blot of TGFβ1 phosphorylated SMAD3 (S423/S425) and phosphorylated p38 (T180/Y182) in co-cultured IHH hepatocytes with different colorectal cancer cell lines. The bottom panel represents the intensity of TGFβ1 bands ($n = 3$). **c** TGFβ1 immunofluorescence staining of IHH hepatocytes co-cultured with various cancer cell lines. **d, e** Immunoblotting represents TGFβ1 expression in co-cultured IHH hepatocytes with HT29 or SW620 cancer cells expressing either shRNA-Scrambled or shRNA-RUNX1 (top panel). The bottom panel represents the intensity of TGFβ1 bands ($n = 3$). **f, g** Immunoblotting showing TSP1 expression in HT29 and SW620 cancer cells, respectively in the presence or absence of shRNA-RUNX1 (top panel). Bottom panels represent the intensity of TSP1 bands ($n = 3$). **h** The top panel shows immunohistochemical staining of chemo-naïve CRCLM lesions with TSP1 antibody. The bottom panel represents quantification of TSP1 positivity [total number of positive pixels/total number of pixels] that measured in RHGP ($n = 5$) and DHGP ($n = 5$) lesions using an optimized Aperio algorithm (mean \pm SD). A-RHGP=Adjacent hepatocytes to tumor lesion in RHGP, C-RHGP=Central tumor cells in RHGP, P-RHGP=Peripheral tumor cells in RHGP, A-DHGP=Adjacent hepatocytes to tumor lesion in DHGP, C-DHGP=Central tumor cells in DHGP, P-DHGP Peripheral tumor cells in DHGP. **i** Immunoblotting shows TGFβ1 expression in the IHH hepatocyte cell line upon TSP1 treatment (top panel). The bottom panel represents the intensity of TGFβ1 bands ($n = 3$). **j** Immunoblotting shows TGFβ1 expression in co-cultured IHH hepatocytes with colorectal cancer (HT29 and LS174) cells expressing either shRNA-Scrambled or shRNA-TSP1 (top panel). The intensity of the bands was quantified using ImageJ and represented as a fold change (bottom panels), $n = 3$ independent experiments. **k** Schematic of experimental strategy (top panel). The bottom left panel shows the Western blot of RUNX1 in colorectal cancer (HT29, SW620, and COLO320dm) cells cultured either individually or co-cultured with hepatocyte (IHH) cell line. The intensity of the bands of RUNX1 was quantified using ImageJ and represented as a fold change, $n = 3$ independent experiments. The bottom right panel is representative of a Western blot showing the abundance of TGFβ1 in the condition media of colorectal cancer (HT29, SW620, and COLO320dm) cells cultured either individually or co-cultured with IHH hepatocytes. Ponceau staining was used as a loading control. **l** Western blot of RUNX1, SMAD3 (S423/S425), and phosphorylated p38 (T180/Y182) in HT29 cells co-cultured hepatocyte (IHH) cells in the presence or absence of LSKL treatment (left panel). The bottom panel shows the intensity of RUNX1 bands ($n = 3$). Data are presented as the mean \pm SD.

that vessel co-option is the main alternative vascularization pathway that could drive anti-angiogenic therapy resistance^{11,12,14}. Of note, vessel co-option vascularization is primarily linked to replacement subtype CRCLM tumors^{11,14}. The mechanistic pathways by which vessel co-option occurs in CRCLMs are poorly understood. Various studies reported that cancer cells in co-opted tumors are characterized by higher levels of motility^{9,11,12,14,20,29}. In this context, a recent study from our lab demonstrated that knockdown of the ARP2/3 subunit ARPC3 attenuates vessel co-option in CRCLMs¹⁴. However, further investigation is required to identify the molecular pathways that regulate ARP2/3 expression, as well as the role of crosstalk between the normal liver and cancer cells in the replacement HGP.

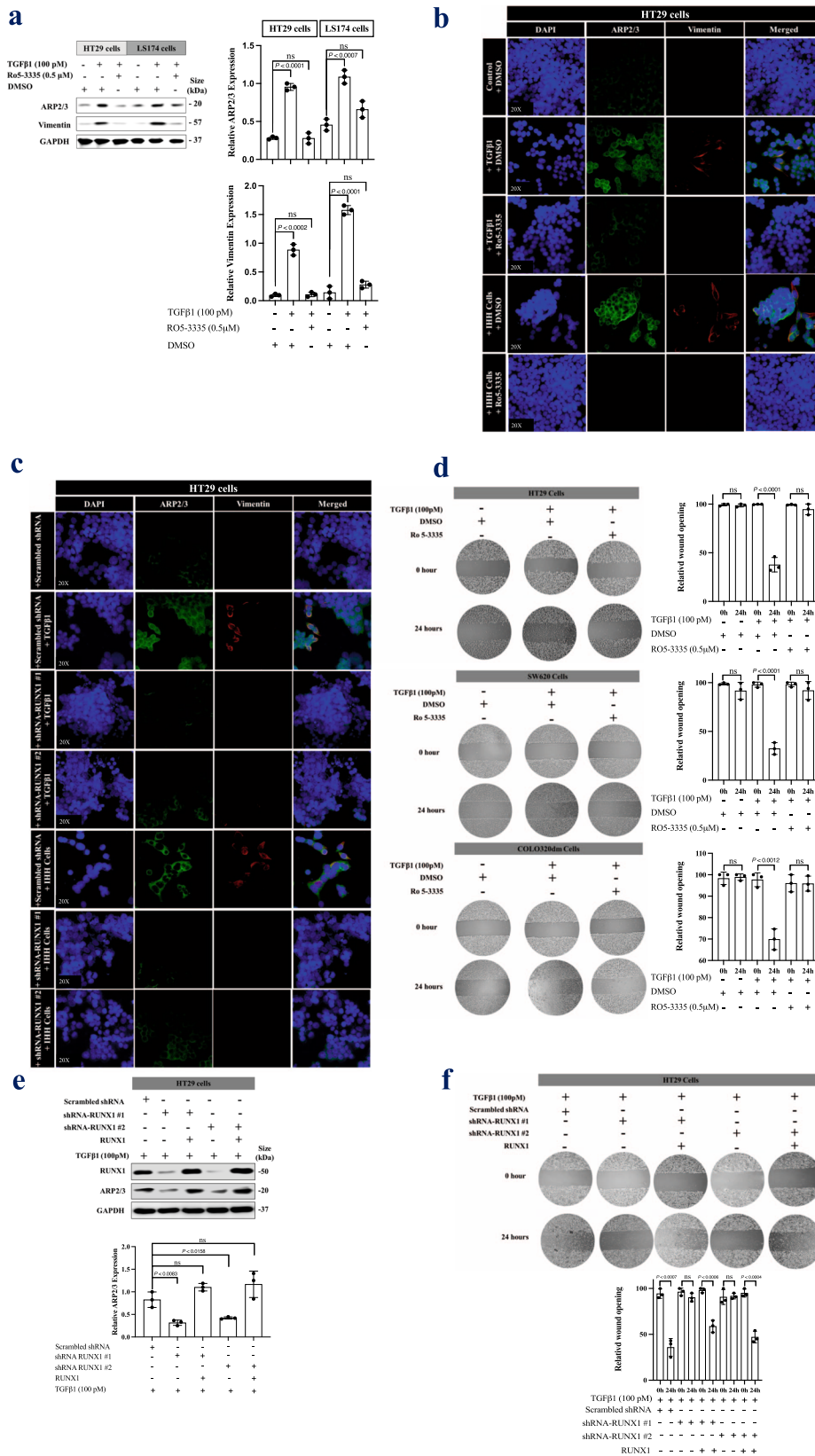
The role of RUNX1 in angiogenesis is controversial to some extent. In this context, RUNX1 has been reported as a pro-angiogenic protein^{84–87}. Mice deficient in RUNX1 die as embryos or soon after birth with a defect in definitive hematopoiesis⁸⁸. On the other hand, various studies demonstrated RUNX1 blocks angiogenesis through repression of VEGF expression^{89–91}. Moreover, Lirdprapamongkol et al.⁹² have reported RUNX1 as one of the molecules that upregulated in the tumor cells in vasculogenic mimicry lesions in hepatocellular carcinoma, while it is not clear how RUNX1 orchestrates the vasculogenic mimicry. Vasculogenic mimicry is a non-angiogenic phenotype where cancer cells mimic endothelial cells by forming blood vessel-like structures that are perfused via connection to the host vasculature¹⁰. In this study, we found the role of RUNX1 in vessel co-option. Our data suggested RUNX1 as an upstream transcriptional regulator of ARP2/3 in metastatic colorectal cancer cells in liver metastases. In agreement with our results, other studies suggested RUNX1 as a positive regulator of ARP2/3^{31–33}, which controls the expression of various subunits including ARPC1, ARPC2, and ARPC3³⁴. It is noteworthy that TGFβ1 family has been reported as a regulator of RUNX1^{48,93–95}. TGFβ1 is among TGFβ members that modulate RUNX1 expression in cancer cells⁹⁶. In agreement with these findings, we demonstrated an increase of RUNX1 expression upon TGFβ1 treatment.

TGFβRII is a well-established receptor for TGFβ1 that is associated with poor prognosis in various cancers, such as metastatic breast cancer⁹⁷, colorectal cancer⁹⁸, and prostate cancer⁹⁹. Importantly, TGFβRII has been identified as an

essential mediator of TGFβ1-dependent RUNX1 expression¹⁰⁰. Similarly, we observed that the knockdown of TGFβRII diminishes the function of TGFβ1 towards RUNX1 expression in colorectal cancer cells.

RUNX1 is known as a transcriptional regulator of *THBS1* that encodes the TSP1 protein^{56,101}, which is highly expressed in replacement type CRCLM tumors (GSE151165)⁴⁰. TSP1 is an anti-angiogenic protein^{102,103} that fulfills a plethora of biological functions and its overexpression is associated with invasive and metastatic phenotypes in various cancers, for instance, glioblastoma²⁹, prostate cancer¹⁰⁴, and medulloblastoma¹⁰⁵. Pleiotropic effects of TSP1 are exerted by its binding to diverse receptors including CD47, CD36, LRP1, and integrin α3β1¹⁰⁶. CD36 is among the TSP1 receptors involved in TSP1-dependent TGFβ1 expression and activation^{63–65}. Our results showed overexpression of CD36 in the hepatocytes of replacement CRCLM lesions; specifically, those bordering the cancer cells. However, future experiments will be needed to gain information on other TSP1 receptors (e.g., CD47, LRP1, and integrin α3β1) and identify their role in CRCLM vessel co-option. Similar to CD36, high expression of TGFβ1 was found in the hepatocytes adjacent to cancer cells compared to distal hepatocytes. This phenomenon supports the possibility that TSP1 may be responsible for TGFβ1 upregulation in the hepatocytes of the co-opted CRCLM sections, and CD36 seems to play a key role in this process. Indeed, our in vitro data also confirmed the importance of TSP1 for TGFβ1 expression in hepatocytes. The outcome of this study suggests a positive feedback loop between TGFβ1 and RUNX1, mediated via TSP1 (Fig. 6).

In this study, we mainly focused on the role of RUNX1 in chemo-naïve CRCLM patients. However, we also observed significant upregulation of RUNX1 in the cancer cells of replacement HGP CRCLM lesions that are typically resistant to the combination of chemotherapy with bevacizumab (Chemo + bev) (Supplementary Fig. 1a). These data indicate that RUNX1 likely contributes to therapy resistance in CRCLM patients. RUNX1 has been associated with anti-cancer therapy resistance through PI3-kinase/Akt pathways in Acute megakaryoblastic leukemia (AMKL) individuals without Down syndrome (non-DS-AMKL)¹⁰⁷. Likewise, the aberrant elevation of Runt-related transcription factor 2 (RUNX2) positively correlated with anti-cancer resistance in various cancers, such as osteosarcomas, breast cancer, and pancreatic cancer^{108–110}.



In this study, we discovered the role of RUNX1 in vessel co-option. Although we presume that these results are mainly due to reduced ARP2/3-dependent cancer cell invasion¹⁴, decreasing the expression of anti-angiogenic genes that are regulated by RUNX1 (e.g., Ang1 and IGFBP3) may have played a role as well. Therefore, more studies are needed to explore the role of anti-

angiogenic genes regulated by RUNX1 in the development of vessel co-opting CRCLM tumors.

In conclusion, this study revealed that RUNX1 plays an essential role in the development of replacement pattern vessel co-opting CRCLM lesions through regulation of its downstream molecules including ARP2/3, vimentin, and TSP1, which facilitate

Fig. 4 TGFβ1 promotes cancer cells motility through RUNX1. **a** Western blot of ARP2/3 and vimentin expression in HT29 or LS174 cells upon exposure to recombinant TGFβ1 (left panel). The right panel represents the intensity of ARP2/3 and vimentin bands ($n = 3$). **b** Immunofluorescence staining of colorectal HT29 cancer cells showing the effect of RUNX1 inhibitor (Ro5-3335, 0.5 μM) on the expression of ARP2/3 (green) and vimentin (red) in the presence of TGFβ1 (100pM) or co-cultured hepatocyte (IHH) cell line. **c** Immunofluorescence staining of ARP2/3 (green) and vimentin (red) in colorectal cancer (HT29) cells expressing either scrambled or RUNX1 shRNA. The cells were either treated with TGFβ1 (100pM) or co-cultured with a hepatocyte (IHH) cell line for 24 h. **d** Representative scratch assay in colorectal cancer (HT29, SW620, and COLO320dm) cells upon treatment with TGFβ1 (100pM) individually or combined TGFβ1 (100pM) plus RUNX1 inhibitor (Ro5-3335, 0.5 μM). **e** Immunoblotting showing ARP2/3 expression in RUNX1-silenced HT29 cancer cells expressing ectopic RUNX1 (top panel). The intensity of the bands was quantified using ImageJ and represented as a fold change. $n = 3$ independent experiments (bottom panel). **f** Scratch assay showing the rescue effects of RUNX1 in HT29 cancer cells invasion. Data are presented as the mean ± SD.

cancer cell motility. Also, we discovered a positive feedback loop between TGFβ1 and RUNX1, mediated by TSP1, which possibly has a potential implication for new strategies to overcome resistance to anti-angiogenic therapy.

Methods

Patient samples. The study was conducted in accordance with the guidelines approved by McGill University Health Centre Institutional Review Board (IRB). Informed consent was obtained from all patients through the McGill University Health Centre (MUHC) Liver Disease Biobank. Surgical specimens were procured and released to the Biobank immediately after the pathologist's confirmation of carcinoma and surgical margins.

Cell cultures. Human colorectal cancer (HT29, LS174, LS180, SW620, COLO320dm) cell lines were a gift kindly supplied by Dr. Alex Alex Gregorieff (Cancer Research Program, McGill University). HCT116 and HEK293T packaging cells were kindly provided by Dr. Daniela Quail and Dr. Peter Siegel, respectively (Rosalind and Morris Goodman Cancer Research Centre, McGill University). IHH cells were a generous gift from Dr. Nabil G. Seidah at Montreal Clinical Research Institute (IRCM). The cells were cultured in DMEM (Wisent Inc., #319-005-CL) supplemented with 10% FBS (Wisent Inc., #085-150) and 1× penicillin/streptomycin (Wisent Inc., 450-201-EL). All cells were cultured at 37 °C with 5% CO₂.

Cells were treated with various inhibitors including ITD1 (Tocris, #5068), LSKL1 (AnaSpec, #AS-60877), and Ro5-3335 (Millipore, #219506).

Co-culture, treating cells with recombinant TGFβ1 or TSP1. Before experiments with recombinant TGFβ1 (PeproTech, # 100-21) or TSP1 (Sigma Aldrich, #ECM002-50UG), the cells were seeded in DMEM (Wisent Inc., #319-005-CL) supplemented with 10% FBS (Wisent Inc., #085-150) and 1× penicillin/streptomycin (Wisent Inc., 450-201-EL) overnight. The next day, the conditioned media was aspirated, and the cells were washed with PBS (Wisent Inc., #311-010-CL) twice. Then, serum-free DMEM supplemented with either TGFβ1 or TSP1 was added and the cells were incubated for 24 h at 37 °C. Co-culturing was conducted using 6-well inserts (Falcon, #353090) and companion plates (Falcon #353502). The cells were cultured with DMEM (Wisent Inc., #319-005-CL) supplemented with 10% FBS (Wisent Inc., #085-150) and 1× penicillin/streptomycin (Wisent Inc., 450-201-EL) overnight. The next day, the media was removed, and the cells were washed twice with PBS (Wisent Inc., #311-010-CL). New serum-free DMEM (Wisent Inc., #319-005-CL) was added and incubated at 37 °C for 24 h.

Immunoblotting. Immunoblotting was performed following the previously published protocols^{111–114}. Briefly, cells were washed once with 1× PBS, trypsinized, collected, and kept on ice. Cells were ruptured by passing through a syringe 10 times and centrifuged for 10 min at 5000 rpm. The supernatant was transferred into 1.5 mL microcentrifuge tubes, and protein concentrations were determined using BCA Protein Assay Kit (Thermo Scientific, #23225). 5–10 μg of total protein per sample were subjected to 10–12% SDS-PAGE and transferred to Immobilon-E membranes (Millipore, #IEVH85R). The blots were developed using Pierce ECL Western Blotting Substrate (Thermo Scientific, #32106) and imaged with ImageQuant LAS4000 (GE Healthcare BioScience).

Lysate from frozen CRCLM tumor lesions was prepared by chopped the tumor tissues into small pieces and transferred them to a tube containing lysis buffer (100 mM Tris-HCl pH 8.0, 150 mM NaCl, 1% Triton X-100, 2 mM EDTA, 1 mM PMSF, protease inhibitor cocktail and double-distilled H₂O). The cells were homogenized on ice using a tissue grinder and incubated for 30 min on ice. The samples were spun down at 15000 × *g* for 30 min and the supernatant was transferred to a fresh tube and another centrifuge was performed at 15,000 × *g* for 30 min. The supernatant was transferred to a fresh tube and used for Western blotting following the protocol. The intensity of the bands was measured using ImageJ (NIH, Bethesda, MD) software^{111,115}. The uncropped blot images are shown in Supplementary Fig. 9.

The following primary antibodies were used: GAPDH 1:2000 (Abcam, #ab9485), TGFβ1 1:200 (Santa Cruz, #sc-130348), Phosphorylated p38 (Thr180/Tyr182) 1:500 (Cell Signaling Technology, #4631), Phosphorylated SMAD3 (Ser423/425) 1:1000 (abcam, #ab52903), RUNX1 1:500 (LS Bio, #LS-C353932), ARP2/3 1:1000 (Millipore, #MABT95), Vimentin 1:1000 (abcam, ab16700), TGFβRII 1:1000 (Thermo Fisher, #PA5-35076), Ang1 1:1000 (abcam, #ab102015) and IGFBP3 1:1000 (Proteintech, #10189-2-AP).

Immunohistochemical staining. Formalin-fixed paraffin-embedded (FFPE) CRCLM resected blocks were used for this study. Serial sections 4 mm thick were cut from each FFPE block, mounted on charged glass slides (Fisher Scientific, #12-550-15), and baked at 37 °C overnight. Prior to staining, the slides were baked at 60 °C for 1 h as well. Hematoxylin and eosin (H&E)-stained sections were prepared from all cases for an initial histopathological assessment. The sections were deparaffinized with xylene (Leica, #3803665) followed by hydration with graded concentrations of ethanol (Comal, #P016EAAN) and then with distilled water. Samples were subjected to antigen retrieval followed by washing with PBS and incubation in hydrogen peroxide (Dako, #S2003) to inhibit endogenous peroxidase. The tissue sections were blocked with 1% goat serum and incubated with the indicated primary antibody in 1% goat serum overnight at 4 °C. After washing, the sections were incubated with secondary antibody (Dako, Anti-Mouse: #K4001; Anti-Rabbit: #K4003) for 1 h at room temperature and positive signals were visualized with the diaminobenzidine (DAB) substrate (Dako, #K3468). The following primary antibodies were used: TGFβ1 1:1500 (Abcam, #ab27969), TGFβ1 1:100 (Abcam, #ab215715), RUNX1 1:200 (LS Bio, #LS-C353932), E-Cadherin 1:200 (R&D systems, #MAB1838-100), TGFβRII 1:200 (Thermo Fisher, #PA5-35076), CD36 1:200 (abcam, #ab133625), TSP1 1:200 (abcam, #ab1823), CBFβ 1:100 (LSBio, #LS-C342588), ARP2/3 1:300 (Millipore, #MABT95; Bioss, #bs-12524R) and Ang1 1:50 (Abcam, #ab215715).

All slides were scanned at ×20 magnification using the Aperio AT Turbo system. Images were viewed using the Aperio ImageScope ver.11.2.0.780 software program for scoring analysis and assessment of signals. The positivity [Total number of positive pixels divided by the total number of pixels: (NTotal - Nn)/(NTotal)] was assessed with an Aperio ScanScope (Aperio Technologies Inc., Vista, CA)^{11,12}.

Immunofluorescence staining. Formalin-fixed paraffin-embedded (FFPE) human CRCLM resected blocks were deparaffinized with xylene followed by hydration with graded concentrations of ethanol and then with distilled water. Samples were subjected to antigen retrieval followed by washing with PBS and incubation in hydrogen peroxide (Dako, #S2003) to inhibit endogenous peroxidase. The tissue sections were blocked with 1% goat serum and incubated with the indicated primary antibody in 1% goat serum overnight at 4 °C. After washing, the sections were incubated with secondary antibody 1:1000 (Alexa Flour 594 goat anti-rabbit IgG and Alexa Flour 488 goat anti-mouse IgG (Invitrogen #A11037 and #A10680, respectively)) for 1 h at room temperature followed by washing thrice. The sections were incubated with 4',6-Diamidino-2-Phenylindole, Dihydrochloride DAPI 1:1000 (Thermo Fisher Scientific, D1306) in PBS for 10 min at room temperature. Prior to mounting undercover glasses, 1–2 drops of ProLong Gold Antifade Mountant (Thermo Fisher Scientific, P36934) were added to each section.

Immunofluorescence staining for cells was performed following the protocol^{115–117}. Briefly, the cells were fixed with 4% paraformaldehyde (Biolegend, #420801), washed with PBS, and permeabilized with 0.1% Triton X-100 (Bio-Rad, #161-0407).

The cells were then washed with PBS and blocked with 1% BSA (GE Healthcare Life Science, #SH30574.02) followed by incubation with primary antibody at 4 °C overnight. The following day, cells were washed with PBS and incubated with 100 μl of 1:1000 secondary antibodies for 1 h in the dark. After incubation, coverslips were washed three times with PBS and stained with DAPI 1:1000 for 10 min. The coverslips were mounted on slides using ProLong Gold Antifade Mountant (Thermo Fisher Scientific, P36934). Slides were visualized using a Zeiss LSM780 confocal microscope system. The following primary antibodies were used: TGFβ1 1:1500 (Abcam, #ab27969), Phospho-p38 1:50 (Thr180/Tyr182) (Cell Signaling Technology, #4631), TSP1 1:200 (abcam, #ab1823), ARP2/3 1:300 (Millipore, #MABT95), Vimentin 1:200 (abcam, ab16700), Phospho-Smad2 1:200 (Ser465/

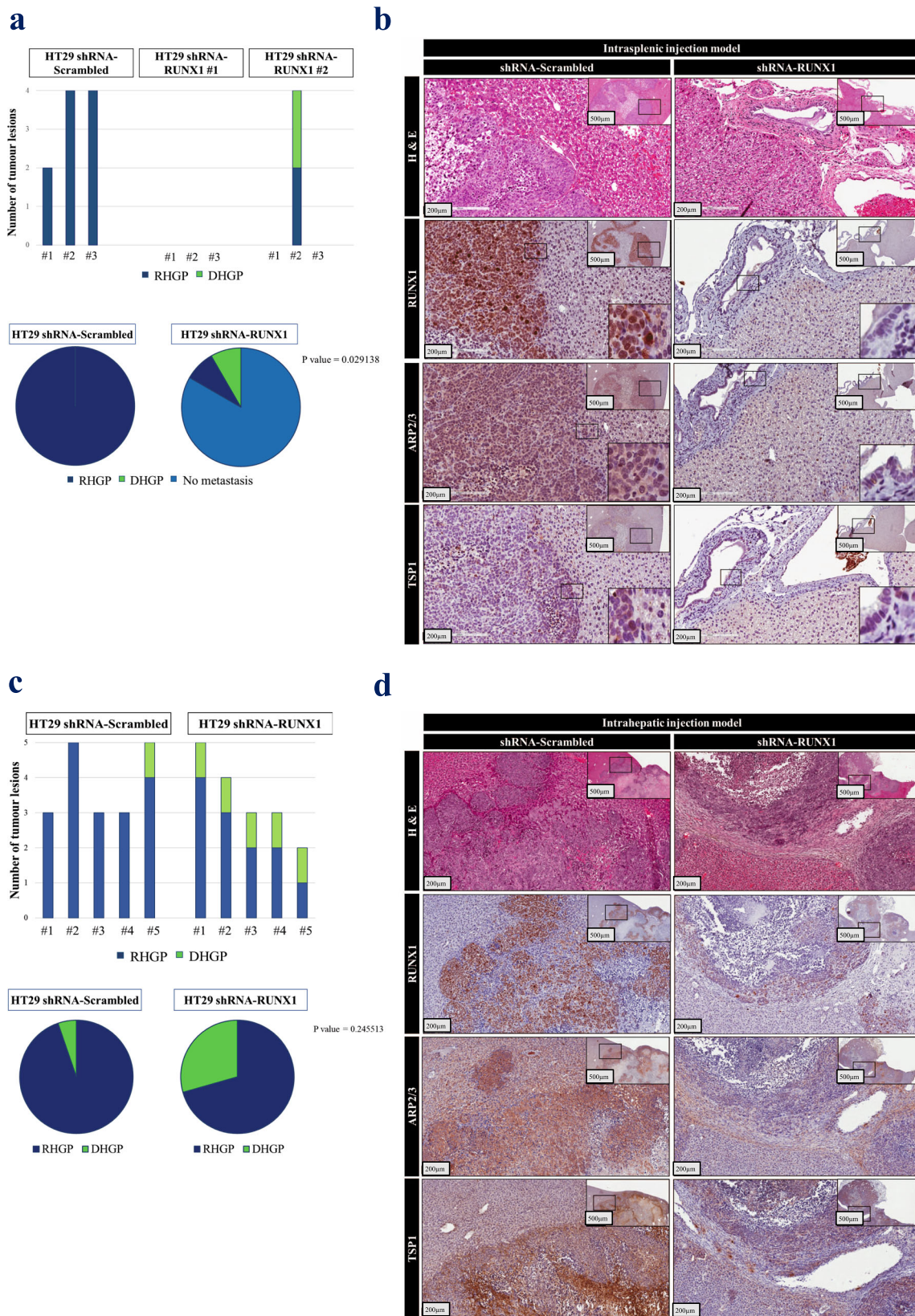


Fig. 5 Silencing RUNX1 in CRC cells attenuated their capability for metastasis and development of co-opted lesions in vivo. **a** Represents number (top panel) and ratio (bottom panel) of hepatic tumor lesions that developed from intrasplenically injected mice with control or RUNX1-depleted HT29 cancer cells. *P* values were calculated using the Chi-square test. **b** Represents H&E and immunohistochemical staining of metastatic tumor sections. **c** The number (top panel) and ratio (bottom panel) of developed hepatic tumor lesions from intrahepatically injected mice by both control and RUNX1-depleted HT29 cells are shown. *P* values were calculated using the Chi-square test. **d** Represents H&E and immunohistochemical staining of tumor sections.

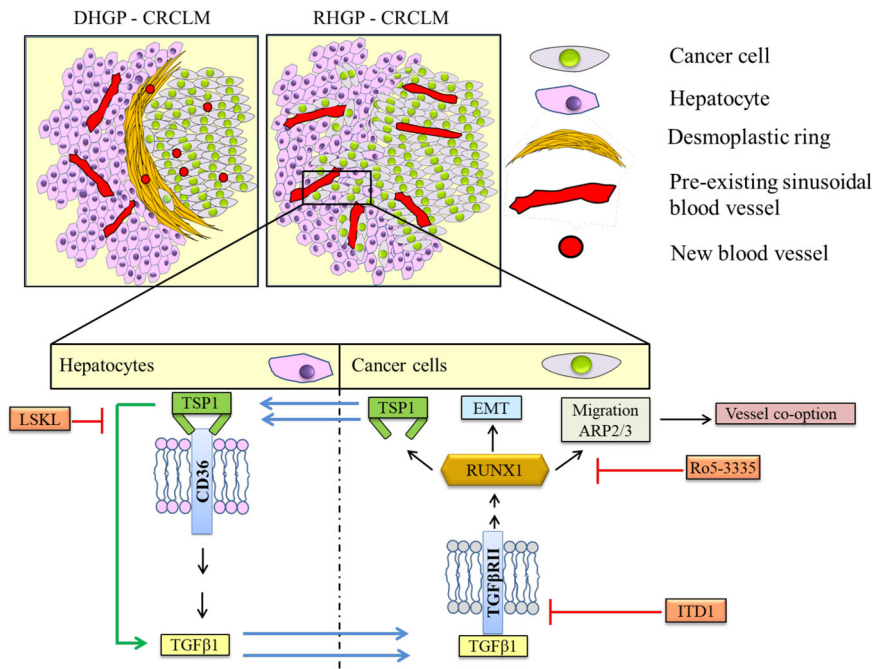


Fig. 6 Proposed model of RUNX1 signaling in co-opted CRCLM lesions. Schematic representation of key findings in our study. RUNX1 plays a central role in the development of vessel co-option in CRCLM. RUNX1 overexpression results in the expression of its target genes that contribute to cancer cells motility and EMT. TSP1 is one of the RUNX1 target genes that are expressed and secreted by cancer cells, which modulates the expression and activity of TGF β 1 in the hepatocytes in the normal adjacent liver. The secreted TGF β 1 by adjacent hepatocytes contributes to RUNX1 overexpression in the peripheral cancer cells through TGF β RII. Consequently, RUNX1 forms a positive feedback loop with TGF β 1 through TSP1.

467) (Cell Signaling Technology, #3101), Cytokeratin 20 1:100 (abcam, #ab76126), Ang1 1:1000 (abcam, #ab102015), IGFBP3 1:200 (Proteintech, #10189-2-AP) and HSA 1:300 (Santa Cruz, #SC5893).

Fluorescence in situ hybridization (FISH). To identify TGF β 1 expression in CRCLM lesions fluorescence in situ hybridization was performed according to the manufacturer's recommendations using RNAscope Probe-Hs-TGF β 1, labeled with Alexa 488 nm fluorescent dye¹². Briefly, formalin-fixed paraffin-embedded (FFPE) human CRCLM sections (4 μ m) were baked for 1 h at 60 °C. The sections were deparaffinized through successive baths of xylene (100%), ethanol (95%), and then distilled water. After drying, the slides were incubated for 10 min with RNAscope Hydrogen Peroxide at room temperature followed by washing. Then, target retrieval was conducted by incubating the slides with RNAscope 1 \times Target Retrieval Reagents in a steamer for 20 min. The sections were incubated with ethanol for 3 min, dried, and incubated with RNAscope Protease Plus at Incubate at 40 °C for 30 min. The slides were washed, dried, and Hybridization was carried out with RNAscope Probe-Hs-TGF β 1-C2 (ACDBIO, #400881-C2) diluted in a Blank Probe-C1 (ACDBIO, #300041) and incubated in HybEZTM Oven (ACDBIO, #321710) at 40 °C for 2 h. The slides were then incubated with SSC buffer (Sigma-Aldrich/MLS, #S6639-1L) overnight at room temperature. The next day, the slides were washed and incubated at 40 °C with RNAscope Multiplex FL V2 AMP-1 (ACDBIO, #323110) for 30 min, RNAscope Multiplex FL V2 AMP-2 for 30 min and RNAscope Multiplex FL V2 AMP-3 for 15 min. After washing, the sections were incubated with RNAscope Multiplex FL v2 HRP-C1 (ACDBIO, #323110) for 15 min at 40 °C. The dye was prepared by diluting Opal 520 Reagent in RNAscope Multiplex TSA Buffer 1:1500 (ACDBIO, #322809) and added to the sections for 30 min at 40 °C followed by incubation with RNAscope[®] Multiplex FL v2 HRP blocker for 15 min at 40 °C. Next, we incubate the slides in 1% BSA for 30 min at room temperature and staining was performed with Cytokeratin-20 1:100 (abcam, #ab76126) following the abovementioned Immunofluorescence staining protocol. The sections were mounted under coverslip using ProLong Gold Antifade Mountant (Thermo Fisher Scientific, P36934) and visualized with Zeiss LSM780 confocal microscope system.

Lentiviral shRNA knockdown. RUNX1, TSP1 TGF β RII knockdown was achieved using lentiviral shRNA vectors from the Mission TRC genome-wide shRNA collections purchased from Sigma-Aldrich Corporation with the following catalog numbers; Scrambled shRNA#: SHC016, RUNX1#1: TRCN0000338428, RUNX1#2: TRCN0000338427, TSP1#1: TRCN0000226402, TSP1#2: TRCN0000219072, TGF β RII#1: TRCN0000000831 and TGF β RII#2: TRCN0000000834. Lentiviral supernatants were generated using the calcium phosphate method as described¹¹⁸. Cancer cells were incubated with lentivirus-containing media with polybrene (8 μ g/ml) and incubated

for 72 h at 37 °C with 5% CO₂ followed by 1 μ g/ml of Puromycin (Wisent Inc., 450-162-XL) selection for 15 days.

Co-immunoprecipitation (Co-IP). Co-immunoprecipitation (Co-IP) was conducted following the protocol^{115,117}. Hepatocyte (IHH) cancer cells were cultured at 37 °C for 24 h in DMEM media supplemented with 10% FBS and 1% 1 \times penicillin/streptomycin. The next day, the media was replaced with new serum-free DMEM media supplemented with recombinant TSP1 (Sigma Aldrich, #ECM002-50UG) for 24 h. The treated cells were collected and lysed. The extract solution was divided into three parts as follows: 10% as input, 45% for immunoprecipitation with anti-IgG antibody (Santa Cruz, #sc-2025), and 45% for immunoprecipitation with anti-CD36 antibody (abcam, #ab133625). 1 μ g of the desired antibody was added to the extract solution and incubated overnight at 4 °C in the rotator. Concurrently, the beads (Millipore, #16-157) were blocked by mixing with 5% BSA and incubating overnight at 4 °C with rotation. The next day, the blocked beads were incubated with the lysate-antibody mixture for 4 h at 4 °C with rotation. Bound proteins were analyzed by Western blotting.

Scratch assay. Before the experiments, the plates were coated with poly-L-Lysine (Millipore, #A-005-CL) and incubated for 30 min at 37 °C, followed by aspiration and air-drying. The cancer cells were seeded overnight using DMEM (Wisent Inc., #319-005-CL) supplemented with 10% FBS (Wisent Inc., #085-150) and 1 \times penicillin/streptomycin (Wisent Inc., 450-201-EL). The media was aspirated, and a wound was introduced into the monolayer cells using a p200 pipette tip. After washing with PBS (Wisent Inc., #311-010-CL), the denuded areas were photographed (0 h). Cells were then cultured using serum-free media for 24 h at 37 °C. The cells were washed, and the scratched areas were photographed (24 h)¹². The relative wound opening was assessed using ImageJ (NIH, Bethesda, MD) software^{119,120}.

Proliferation assay. We performed this assay to determine the effect of RUNX1 on proliferation rates in HT29. A similar number of HT29 cells expressing either shRNA-Scrambled or shRNA-RUNX1 were cultured in DMEM (Wisent Inc., #319-005-CL) supplemented with 10% FBS (Wisent Inc., #085-150), 1 \times penicillin/streptomycin (Wisent Inc., 450-201-EL) and 1 μ g/ml of Puromycin (Wisent Inc., 450-162-XL) at 37 °C. Every 12 h the cells were collected by trypsinization followed by counting using trypan blue (Bio-Rad, #1450021).

Xenograft experiments. To identify the role of RUNX1 on the histological growth pattern of CRCLM, we performed both intrasplenic and intrahepatic mouse model experiments. The mice were randomly assigned to each group. Colorectal cancer liver metastases were generated in 4-week to 6-week old SCID Beige mice by

intrasplenic injection of 50 μ L of PBS (Wisent Inc., #311-010-CL) containing 1×10^6 HT29 shRNA-Scrambled, HT29 shRNA-RUNX1 #1, or HT29 shRNA-RUNX1 #2 followed by splenectomy 1 min after injection¹². Mice were euthanized 6 weeks later. We also conducted intrahepatic injection to further validate the role of RUNX1 in vivo. 1×10^6 HT29 (Scrambled or shRNA-RUNX1) colorectal cancer cells were injected into the liver of 4-week to 6-week old SCID Beige mice. All animals were monitored daily for survival until the experimental endpoint. After 6 weeks, the mice were sacrificed.

Next, sections of the liver were collected and fixed in 10% buffered neutral formalin, and paraffin-embedded. Hematoxylin and eosin (H&E)-stained sections were prepared from all samples for an initial histopathological assessment. The mice were housed in facilities managed by the McGill University Animal Resources Centre. All animal experiments were conducted under a McGill University-approved Animal Use Protocol in accordance with guidelines established by the Canadian Council on Animal Care.

Statistical reproducibility. Statistical analysis was performed with a two-tailed Student's *t*-test using GraphPad Prism software version 7.0 (GraphPad Software, La Jolla, CA, USA) and Excel software. Data presented as mean \pm standard deviation. Unpaired Student's *t*-test was applied to compare the means of two groups. The association between the two categorical groups in xenograft experiments was assessed with the Chi-square test. *P*-values of <0.05 were considered to be significant.

Reporting summary. Further information on research design is available in the Nature Research Reporting Summary linked to this article.

Data availability

RNA-seq data are publicly available in GEO with the accession (GSE151165). The datasets generated and/or analyzed during this study can be found in Supplementary Data 1. All other relevant data are available from the corresponding author upon reasonable request.

Received: 31 July 2020; Accepted: 17 June 2021;

Published online: 10 August 2021

References

- Bray, F., Ferlay, J. & Soerjomataram, I. Global Cancer Statistics 2018: GLOBOCAN estimates of Incidence and Mortality Worldwide for 36 cancers in 185 countries. *Ca. Cancer J. Clin.* **68**, 394–424 (2018).
- Zarour, L. R. et al. Colorectal cancer liver metastasis: evolving paradigms and. *Cell. Mol. Gastroenterol. Hepatol.* **3**, 163–173 (2017).
- Tomlinson, J. S. et al. Actual 10-year survival after resection of colorectal liver metastases defines cure. *J. Clin. Oncol.* **25**, 4575–4580 (2007).
- Fusai, G. & Davidson, B. R. Strategies to increase the resectability of liver metastases from colorectal cancer. *Dig. Surg.* **20**, 481–496 (2003).
- Kerbel, R. S. Tumor angiogenesis. *N. Engl. J. Med.* **358**, 2039–2049 (2008).
- Ferrara, N., Hillan, K. J., Gerber, H., Novotny, W. & Francisco, S. S. Discovery and development of bevacizumab, an anti-VEGF antibody for treating cancer. *Nat. Rev. Drug Discov.* **3**, 391–400 (2004).
- Cunningham, D. et al. Bevacizumab plus capecitabine versus capecitabine alone in elderly patients with previously untreated metastatic colorectal cancer (AVEX): an open-label, randomised phase 3 trial. *Lancet Oncol.* **14**, 1077–1085 (2013).
- Hurwitz, H. et al. Bevacizumab plus irinotecan, fluorouracil, and leucovorin for metastatic colorectal cancer. *N. Engl. J. Med.* **350**, 2335–2342 (2004).
- Kuczynski, E. A., Vermeulen, P. B., Pezzella, F., Kerbel, R. S. & Reynolds, A. R. Vessel co-option in cancer. *Nat. Rev. Clin. Oncol.* **16**, 469–493 (2019).
- Vasudev, N. S. & Reynolds, A. R. Anti-angiogenic therapy for cancer: current progress, unresolved questions and future directions. *Angiogenesis* **17**, 471–494 (2014).
- Lazaris, A. et al. Vascularization of colorectal carcinoma liver metastasis: insight into stratification of patients for anti-angiogenic therapies. *J. Pathol. Clin. Res.* **4**, 184–192 (2018).
- Ibrahim, N. et al. Angiotensin II deficiency in hepatocytes affects the growth of colorectal cancer liver. *Cancers* **12**, 1–18 (2020).
- Donnem, T. et al. Vessel co-option in primary human tumors and metastases: an obstacle to effective anti-angiogenic treatment? *Cancer Med.* **2**, 427–436 (2013).
- Frentzas, S. et al. Vessel co-option mediates resistance to anti-angiogenic therapy in liver metastases. *Nat. Med.* **22**, 1294–1302 (2017).
- Pezzella, F. et al. Non-small-cell lung carcinoma tumor growth without morphological evidence of neo-angiogenesis. *Am. J. Pathol.* **151**, 1417–1423 (1997).
- Bridgeman, V. L. et al. Vessel co-option is common in human lung metastases and mediates resistance to anti-angiogenic therapy in preclinical lung metastasis models. *J. Pathol.* **241**, 362–374 (2017).
- Pezzella, F. et al. Angiogenesis in primary lung cancer and lung secondaries. *Eur. J. Cancer* **32A**, 2494–2500 (1996).
- Jeong, H. S. et al. Investigation of the lack of angiogenesis in the formation of lymph node metastases. *J. Natl Cancer Inst.* **107**, 1–11 (2015).
- Naresk, K. N., Nerurkar, A. Y. & Borges, A. M. Angiogenesis is redundant for tumour growth in lymph node metastases. *Histopathology* **38**, 466–470 (2001).
- Kuczynski, E. A. et al. Co-option of liver vessels and not sprouting angiogenesis drives acquired sorafenib resistance in hepatocellular carcinoma. *J. Natl Cancer Inst.* **108**, 1–13 (2016).
- Vermeulen, P. B. et al. Liver metastases from colorectal adenocarcinomas grow in three patterns with different angiogenesis and desmoplasia. *J. Pathol.* **195**, 336–342 (2001).
- Dam, P. V. et al. International consensus guidelines for scoring the histopathological growth patterns of liver metastasis. *Br. J. Cancer* **117**, 1427–1441 (2017).
- Rada, M., Lazaris, A., Kapelanski-Lamoureux, A., Mayer, T. Z. & Metrakos, P. Tumor microenvironment conditions that favor vessel co-option in colorectal cancer liver metastases: a theoretical model. *Semin. Cancer Biol.* **71**, 52–64 (2021).
- Nielsen, K., Rolff, H. C., Eefsen, R. & Vanier, B. The morphological growth patterns of colorectal liver metastases are prognostic for overall survival. *Mod. Pathol.* **27**, 1641–1648 (2014).
- Galjart, B. et al. Angiogenic desmoplastic histopathological growth pattern as a prognostic marker of good outcome in patients with colorectal liver metastases. *Angiogenesis* **22**, 355–368 (2019).
- Bohlok, A. et al. Association between the histopathological growth patterns of liver metastases and survival after hepatic surgery in breast cancer patients. *npj Breast Cancer* **6**, <https://doi.org/10.1038/s41523-020-00209-1> (2020).
- Barnhill, R. et al. Replacement and desmoplastic histopathological growth patterns: a pilot study of prediction of outcome in patients with uveal melanoma liver metastases. *J. Pathol. Clin. Res.* **4**, 227–240 (2018).
- Watanabe, K. et al. The “histological replacement growth pattern” represents aggressive invasive behavior in liver metastasis from pancreatic cancer. *Cancer Med.* **9**, 3130–3141 (2020).
- Daubon, T. et al. Deciphering the complex role of thrombospondin-1 in glioblastoma development. *Nat. Commun.* **10**, 1146–1161 (2019).
- Robinson, R. C. et al. Crystal structure of Arp2/3 complex. *Science* **294**, 1679–1684 (2001).
- Lie-a-ling, M. et al. RUNX1 positively regulates a cell adhesion and migration program in murine hemogenic endothelium prior to blood emergence. *Blood* **124**, 11–21 (2014).
- Camos, M. et al. Gene expression profiling of acute myeloid leukemia with rearrangement reveals a distinctive signature with a specific pattern of HOX gene expression. *Cancer Res.* **16**, 6947–6955 (2006).
- Nagase, R. et al. Expression of mutant Asx1 perturbs hematopoiesis and promotes susceptibility to leukemic transformation. *J. Exp. Med.* **215**, 1729–1747 (2018).
- Della Gatta, G. et al. Reverse engineering of TLX oncogenic transcriptional networks identifies RUNX1 as tumor suppressor in T-ALL. *Nat. Med.* **18**, 436–440 (2012).
- Goyama, S. et al. Transcription factor RUNX1 promotes survival of acute myeloid leukemia cells Find the latest version: Transcription factor RUNX1 promotes survival of acute myeloid leukemia cells. *J. Clin. Invest.* **123**, 3876–3888 (2013).
- Sun, C. et al. Expression and prognosis analyses of runt-related transcription factor family in human leukemia. *Mol. Ther. Oncolytics* **12**, 103–111 (2019).
- Mitsuda, Y., Morita, K., Kashiwazaki, G., Taniguchi, J. & Bando, T. RUNX1 positively regulates the ErbB2/HER2 signaling pathway through modulating SOS1 expression in gastric cancer cells. *Sci. Rep.* **8**, 6423–36 (2018).
- Bragt, M. P. A. V., Hu, X., Xie, Y. & Li, Z. RUNX1, a transcription factor mutated in breast cancer, controls the fate of ER-positive mammary luminal cells. *Elife* **3**, 1–23 (2014).
- Eynden, G. G. & Van, den et al. The histological growth pattern of colorectal cancer liver metastases has prognostic value. *Clin. Exp. Metastasis* **29**, 541–549 (2012).
- Palmieri, V. et al. Neutrophils expressing lysyl oxidase-like 4 protein are present in colorectal cancer liver metastases resistant to anti-angiogenic therapy. *J. Pathol.* **251**, 213–223 (2020).
- Škalamera, D. et al. Genome-wide gain-of-function screen for genes that induce epithelial-to-mesenchymal transition in breast cancer. *Oncotarget* **7**, 61000–61020 (2016).
- Liu, Y. et al. PRL-3 promotes epithelial mesenchymal transition by regulating cadherin directly. *Cancer Biol. Ther.* **8**, 1352–1359 (2009).
- Bielasz, B. et al. Epithelial Notch signaling regulates interstitial fibrosis development in the kidneys of mice and humans. *J. Clin. Invest.* **120**, 4040–4054 (2010).
- Zhang, J. et al. Role of ARPC2 in human gastric cancer. *Mediators Inflamm.* **2017**, 1–8 (2017).

45. Song, Y., Ye, M., Zhou, J., Wang, Z. & Zhu, X. Targeting E-cadherin expression with small molecules for digestive cancer treatment. *Am. J. Transl. Res.* **11**, 3932–3944 (2019).
46. Molinie, N. & Gautreau, X. A. The Arp2/3 regulatory system and its deregulation in cancer. *Physiol. Rev.* **98**, 215–238 (2018).
47. Zhou, T. et al. Runt-related transcription factor 1 (RUNX1) promotes TGF- β -induced renal tubular epithelial-to-mesenchymal transition (EMT) and renal fibrosis through the PI3K subunit p110 δ . *Ebiomedicine* **31**, 217–225 (2018).
48. VanOudenhoove, J. J. et al. Transient RUNX1 expression during early mesendodermal differentiation of hESCs promotes epithelial to mesenchymal transition through TGF β 2 signaling. *Stem Cell Rep.* **7**, 884–896 (2016).
49. Wildey, G. M. & Howe, P. H. Runx1 is a co-activator with FOXO3 to mediate transforming growth factor β (TGF β)-induced Bim transcription in hepatic cells. *J. Biol. Chem.* **284**, 20227–20239 (2009).
50. Ábrigo, J. et al. TGF- β requires the activation of canonical and non-canonical signalling pathways to induce skeletal muscle atrophy. *Biol. Chem.* **399**, 253–264 (2018).
51. Rada, M. et al. Cancer cells induce hepatocytes apoptosis in co-opted colorectal cancer liver metastatic lesions. *bioRxiv* **429243**, <https://doi.org/10.1101/2021.02.11.429243> (2021).
52. Willems, E. et al. Small molecule-mediated TGF- β type II receptor degradation promotes cardiomyogenesis in embryonic stem cells. *Cell Stem Cell* **11**, 242–252 (2012).
53. Schippers, I. J. et al. Immortalized human hepatocytes as a tool for the study of hepatocytic (de-)differentiation. *Cell Biol. Toxicol.* **13**, 375–386 (1997).
54. Hang, H. et al. Hepatocyte nuclear factor 4A improves hepatic differentiation of immortalized adult human hepatocytes and improves liver function and survival. *Exp. Cell Res.* **360**, 81–93 (2017).
55. Farra, R. et al. Effects of E2F1 – cyclin E1 – E2 circuit down regulation in hepatocellular carcinoma. *Dig. Liver Dis.* **43**, 1006–1014 (2011).
56. Li, Y. et al. Human NOTCH4 is a key target of RUNX1 in megakaryocytic differentiation. *Blood* **131**, 191–201 (2018).
57. Herglotz, J. et al. Histone arginine methylation keeps RUNX1 target genes in an intermediate state. *Oncogene* **32**, 2565–2575 (2013).
58. Soto-pantoja, D. R. et al. Thrombospondin-1 and CD47 signaling regulate healing of thermal injury in mice. *Matrix Biol.* **37**, 25–34 (2014).
59. Crawford, S. E. et al. Thrombospondin-1 is a major activator of TGF- β 1 in vivo. *Cell* **93**, 1159–1170 (1998).
60. Osz, K., Ross, M. & Petrik, J. The thrombospondin-1 receptor CD36 is an important mediator of ovarian angiogenesis and folliculogenesis. *Reprod. Biol. Endocrinol.* **12**, 21–31 (2014).
61. Chu, L., Ramakrishnan, D. P. & Silverstein, R. L. Thrombospondin-1 modulates VEGF signaling via CD36 by recruiting SHP-1 to VEGFR2 complex in microvascular endothelial cells. *Blood* **122**, 1822–1833 (2013).
62. Pfander, D. et al. Expression of thrombospondin-1 and its receptor CD36 in human osteoarthritic cartilage. *Ann. Rheum. Dis.* **59**, 448–454 (2000).
63. Wang, X., Chen, Y., Lv, L. & Chen, J. Silencing CD36 gene expression results in the inhibition of latent-TGF- β 1 activation and suppression of silica-induced lung fibrosis in the rat. *Respir. Res.* **10**, 36–45 (2009).
64. Hugo, C. The thrombospondin 1 – TGF- β axis in fibrotic renal disease. *Nephrol. Dial. Transpl.* **18**, 1241–1245 (2003).
65. Yehualaeshet, T. et al. Activation of rat alveolar macrophage-derived latent transforming growth factor B-1 by plasmin requires interaction with thrombospondin-1 and its cell surface receptor, CD36. *Am. J. Pathol.* **155**, 841–851 (1999).
66. Breitkopf, K. et al. Thrombospondin 1 acts as a strong promoter of transforming growth factor b effects via two distinct mechanisms in hepatic stellate cells. *Gut* **54**, 673–681 (2005).
67. Liao, F. et al. LSKL peptide alleviates subarachnoid fibrosis and hydrocephalus by inhibiting TSP1-mediated TGF- β 1 signaling activity following subarachnoid hemorrhage in rats. *Exp. Ther. Med.* **12**, 2537–2543 (2016).
68. Wang, H. et al. LIM and SH3 protein 1 induces TGF β -mediated epithelial-mesenchymal transition in human colorectal cancer by regulating S100A4 expression. *Clin. Cancer Res.* **20**, 5835–5847 (2014).
69. Tang, Y. et al. Energetic and functional contribution of residues in the core binding factor β (CBF β) subunit to heterodimerization with CBF α . *J. Biol. Chem.* **275**, 39579–39588 (2000).
70. Cunningham, L. et al. Identification of benzodiazepine Ro5-3335 as an inhibitor of CBF leukemia through quantitative high throughput screen against RUNX1 – CBF β interaction. *Proc. Natl Acad. Sci. USA* **109**, 14592–14597 (2012).
71. Su, X., Wang, S., Huo, Y. & Yang, C. Short interfering RNA-mediated silencing of actin-related protein 2/3 complex subunit 4 inhibits the migration of SW620 human colorectal cancer cells. *Oncol. Lett.* **15**, 2847–2854 (2018).
72. Du, L. et al. High vimentin expression predicts a poor prognosis and progression in colorectal cancer: a study with meta-analysis and TCGA database. *Biomed Res. Int.* **387810**. <https://doi.org/10.1155/2018/6387810> (2018).
73. Takakura, N. et al. A role for hematopoietic stem cells in promoting angiogenesis. *Cell* **102**, 199–209 (2000).
74. Canel, M. et al. Nuclear FAK and Runx1 cooperate to regulate IGFBP3, cell-cycle progression, and tumor growth. *Cancer Res.* **77**, 5301–5312 (2017).
75. Stoeltzing, O. et al. Angiotensin-1 inhibits vascular permeability, angiogenesis, and growth of hepatic colon cancer tumors. *Cancer Res.* **63**, 3370–3377 (2003).
76. Kim, J. H. et al. Antiangiogenic antitumor activities of IGFBP-3 are mediated by IGF-independent suppression of Erk1/2 activation and Egr-1-mediated transcriptional events. *Blood* **118**, 2622–2631 (2011).
77. Thomas, M. et al. A novel angiotensin-2 selective fully human antibody with potent anti-tumoral and anti-angiogenic efficacy and superior side effect profile compared to pan-angiotensin-1/-2 inhibitors. *PLoS ONE* **8**, e54923 (2013).
78. Hendrix, M. J. C., Sefror, E. A., Hess, A. R. & Sefror, R. E. B. Vasculogenic mimicry and tumour-cell plasticity: lessons from melanoma. *Nat. Rev. Cancer* **3**, 411–421 (2003).
79. Hu, Y. et al. Hypoxia-induced autophagy promotes tumor cell survival and adaptation to anti-angiogenic treatment in glioblastoma. *Cancer Res.* **72**, 1773–1783 (2012).
80. Gotink, K. et al. Lysosomal sequestration of sunitinib: a novel mechanism of drug resistance. *Clin. Cancer Res.* **17**, 7337–7346 (2011).
81. Croci, D. O. et al. Glycosylation-dependent lectin-receptor interactions preserve angiogenesis in anti-VEGF refractory tumors. *Cell* **156**, 744–758 (2014).
82. Pinto, M. P., Sotomayor, P., Carrasco-Avino, G., Corvalan, A. H. & Owen, G. I. Escaping antiangiogenic therapy: Strategies employed by cancer cells. *Int. J. Mol. Sci.* **17**, 1–20 (2016).
83. Zarrin, B., Zarifi, F., Vaseghi, G. & Javanmard, S. Acquired tumor resistance to antiangiogenic therapy: mechanisms at a glance. *J. Res. Med. Sci.* **22**, https://doi.org/10.4103/jrms.JRMS_182_17 (2017).
84. Iwatsuki, K. et al. Runx1 promotes angiogenesis by downregulation of insulin-like growth factor-binding protein-3. *Oncogene* **24**, 1129–1137 (2005).
85. Sangpairaj, K. et al. RUNX1 regulates migration, invasion, and angiogenesis via p38 MAPK pathway in human glioblastoma. *Cell. Mol. Neurobiol.* **37**, 1243–1255 (2017).
86. Hamik, A., Wang, B. & Jain, M. K. Transcriptional regulators of angiogenesis. *Arterioscler. Thromb. Vasc. Biol.* **26**, 1936–1947 (2006).
87. Chen, Y. et al. Rasip1 is a RUNX1 target gene and promotes migration of NSCLC cells. *Cancer Manag. Res.* **10**, 4537–4552 (2018).
88. Okuda, T., Van Deursen, J., Hiebert, S. W., Grosveld, G. & Downing, J. R. AML1, the target of multiple chromosomal translocations in human leukemia, is essential for normal fetal liver hematopoiesis. *Cell* **84**, 321–330 (1996).
89. Elst, A. Ter et al. Repression of vascular endothelial growth factor expression by the runt-related transcription factor 1 in acute myeloid leukemia. *Cancer Res.* **71**, 2761–2771 (2011).
90. Lee, S. H. et al. Runx2 protein stabilizes hypoxia-inducible factor-1 α through competition with von Hippel-Lindau protein (pVHL) and stimulates angiogenesis in growth plate hypertrophic chondrocytes. *J. Biol. Chem.* **287**, 14760–14771 (2012).
91. Dowdy, C. R. et al. Definitive hematopoiesis requires Runx1 C-terminal-mediated subnuclear targeting and transactivation. *Hum. Mol. Genet.* **19**, 1048–1057 (2010).
92. Lirdprapamongkol, K., Chiablaem, K., Sila-asna, M. & Surarit, R. Exploring stemness gene expression and vasculogenic mimicry capacity in well- and poorly-differentiated hepatocellular carcinoma cell lines. *Biochem. Biophys. Res. Commun.* **422**, 429–435 (2012).
93. Vogel, T., Ahrens, S., Büttner, N. & Kriegelstein, K. Transforming growth factor β promotes neuronal cell fate of mouse cortical and hippocampal progenitors in vitro and in vivo: Identification of medd9 as an essential signaling component. *Cereb. Cortex* **20**, 661–671 (2010).
94. Vargel, O. et al. Activation of the TGF β pathway impairs endothelial to haematopoietic transition. *Sci. Rep.* **6**, 1–15 (2016).
95. Logan, T. T., Villapol, S. & Symes, A. J. TGF- β superfamily gene expression and induction of the Runx1 transcription factor in adult neurogenic regions after brain injury. *PLoS ONE* **8**, 1–14 (2013).
96. Bogoch, Y. et al. Augmented expression of RUNX1 deregulates the global gene expression of U87 glioblastoma multiforme cells and inhibits tumor growth in mice. *Tumor Biol.* **39**, 1–11 (2017).
97. Meng, X. et al. Myeloid-specific TGF- β signaling in bone promotes basic-FGF and breast cancer bone metastasis. *Oncogene* **35**, 2370–2378 (2016).
98. Zhang, W. et al. MicroRNA-301a promotes migration and invasion by targeting TGFBR2 in human colorectal cancer. *J. Exp. Clin. Cancer Res.* **33**, 1–13 (2014).
99. Li, X. et al. Prostate tumor progression is mediated by a paracrine TGF- β /Wnt3a signaling axis. *Oncogene* **27**, 7118–7130 (2008).
100. Monteiro, R. et al. Transforming growth factor β drives hemogenic endothelium programming and the transition to hematopoietic stem cells. *Dev. Cell* **38**, 358–370 (2016).

101. Glembofsky, A. C. et al. Downregulation of TREM-like transcript-1 and collagen receptor $\alpha 2$ subunit, two novel RUNX1-targets, contributes to platelet dysfunction in familial platelet disorder with predisposition to acute myelogenous leukemia. *Hematologica* **104**, 1244–1255 (2019).
102. Iruela-arispe, M. L., Lombardo, M., Kruttsch, H. C., Lawler, J. & Roberts, D. D. Inhibition of Angiogenesis by Thrombospondin-1 Is Mediated by 2 Independent Regions Within the Type 1 Repeats. *Basic Sci. Rep.* **100**, 1423–1430 (1999).
103. Nör, J. et al. Thrombospondin-1 induces endothelial cell apoptosis and inhibits angiogenesis by activating the caspase death pathway. *J. Vasc. Res.* **37**, 209–218 (2000).
104. Firlej, V. et al. Thrombospondin-1 triggers cell migration and development of advanced prostate tumors. *Cancer Res.* **71**, 7649–7658 (2011).
105. Zhou, L. et al. Silencing of thrombospondin-1 is critical for myc-induced metastatic phenotypes in medulloblastoma. *Cancer Res.* **70**, 8199–8211 (2010).
106. Masli, S., Turpie, B. & Streilein, J. W. Thrombospondin orchestrates the tolerance-promoting properties of TGF β -treated antigen-presenting cells. *Int. Immunol.* **18**, 689–699 (2006).
107. Edwards, H. et al. RUNX1 regulates phosphoinositide 3-kinase/AKT pathway: Role in chemotherapy sensitivity in acute megakaryocytic leukemia. *Blood* **114**, 2744–2752 (2009).
108. Ozaki, T. et al. Impact of RUNX2 on drug-resistant human pancreatic cancer cells with p53 mutations. *BMC Cancer* **18**, 1–15 (2018).
109. Sadikovic, B. et al. Expression analysis of genes associated with human osteosarcoma tumors shows correlation of RUNX2 overexpression with poor response to chemotherapy. *BMC Cancer* **10**, <https://doi.org/10.1186/1471-2407-10-202> (2010).
110. Roos, A. et al. Loss of Runx2 sensitises osteosarcoma to chemotherapy-induced apoptosis. *Br. J. Cancer* **113**, 1289–1297 (2015).
111. Rada, M. et al. Inhibitor of apoptosis proteins (IAPs) mediate collagen type XI alpha 1-driven cisplatin resistance in ovarian cancer. *Oncogene* **37**, 4809–4820 (2018).
112. Ekpenyong-Akiba, A. E. et al. Amelioration of age-related brain function decline by Bruton's tyrosine kinase inhibition. *Aging Cell* **19**, 1–11 (2020).
113. Rada, M., Barlev, N. & Macip, S. BTK modulates p73 activity to induce apoptosis independently of p53. *Cell Death Discov.* **4**, 0–5 (2018).
114. Nallanthighal, S. et al. Inhibition of collagen XI alpha 1-induced fatty acid oxidation triggers apoptotic cell death in cisplatin-resistant ovarian cancer. *Cell Death Dis.* **11**, 1–12 (2020).
115. Rada, M. et al. BTK blocks the inhibitory effects of MDM2 on p53 activity. *Oncotarget* **8**, 106639–106647 (2017).
116. Althubiti, M. et al. BTK modulates p53 activity to enhance apoptotic and senescent responses. *Cancer Res.* **76**, 5405–5414 (2016).
117. Rada, M. et al. Human EHMT2/G9a activates p53 through methylation-independent mechanism. *Oncogene* **36**, <https://doi.org/10.1038/onc.2016.258> (2017).
118. Huang, S. et al. MED12 controls the response to multiple cancer drugs through regulation of TGF- β receptor signaling. *Cell* **151**, 937–950 (2012).
119. Paulo, J., Nunes, S., Abalen, A. & Dias, M. ImageJ macros for the user-friendly analysis of soft-agar and wound-healing assays. *Biotechniques* **62**, 175–179 (2018).
120. Gerlitz, G. & Bustin, M. Efficient cell migration requires global chromatin condensation. *J. Cell Sci.* **123**, 2207–2217 (2010).

Acknowledgements

We thank Dr. Alex Gregorieff (Cancer Research Program, McGill University) and Dr. Nabil Seidah for providing cell lines. We would like to thank Dr. James C. Mulloy's group for providing RUNX1 plasmid. We acknowledge Shaída Ouladan for her support with FISH experiments. We also thank RI-MUHC Liver Disease Biobank for providing CRCLM slides. This work was supported by Dana Massaro and Ken Verdoni Liver Metastases Research Fellowship.

Author contributions

M.R., A.L., P.S., A.R. and P.M. co-conceived the study. M.R. executed the experiments. M.R. performed immunohistochemistry, immunofluorescence, FISH, cell culturing, and immunoblotting. A.K.L. assisted in cell culturing and immunoblotting. S.P. prepared CRCLM samples. S.T. generated RUNX1 knockdown cancer cells and performed xenograft experiments. M.R. wrote the manuscript.

Competing interests

The authors declare no competing interests.

Additional information

Supplementary information The online version contains supplementary material available at <https://doi.org/10.1038/s42003-021-02481-8>.

Correspondence and requests for materials should be addressed to P.M.

Peer review information *Communications Biology* thanks the anonymous reviewers for their contribution to the peer review of this work. Primary Handling Editor: Brooke LaFlamme.

Reprints and permission information is available at <http://www.nature.com/reprints>

Publisher's note Springer Nature remains neutral with regard to jurisdictional claims in published maps and institutional affiliations.



Open Access This article is licensed under a Creative Commons Attribution 4.0 International License, which permits use, sharing, adaptation, distribution and reproduction in any medium or format, as long as you give appropriate credit to the original author(s) and the source, provide a link to the Creative Commons license, and indicate if changes were made. The images or other third party material in this article are included in the article's Creative Commons license, unless indicated otherwise in a credit line to the material. If material is not included in the article's Creative Commons license and your intended use is not permitted by statutory regulation or exceeds the permitted use, you will need to obtain permission directly from the copyright holder. To view a copy of this license, visit <http://creativecommons.org/licenses/by/4.0/>.

© Crown 2021